JOURNAL OF SCIENCE
SAKARYA UNIVERSITY

Sakarya University Journal of Science

ISSN 1301-4048 | e-ISSN 2147-835X | Period Bimonthly | Founded: 1997 | Publisher Sakarya University | http://www.saujs.sakarya.edu.tr/

Title: Electrochemical Corrosion Behavior of High Velocity Oxy-Fuel (HVOF) Superalloy Coatings On Ductile Irons

Authors: Yusuf Kayalı, Muhammet Karabaş, Yılmaz Yalçın, Aysel Büyüksağiş, Şükrü Talaş
Recieved: 2018-09-29 00:00:00
Revised: 2018-11-06 00:00:00
Accepted: 2018-12-14 00:00:00
Article Type: Research Article
Volume: 23
Issue: 2
Month: April
Year: 2019
Pages: 291-300

How to cite
Yusuf Kayalı, Muhammet Karabaş, Yılmaz Yalçın, Aysel Büyüksağiş, Şükrü Talaş; (2019), Electrochemical Corrosion Behavior of High Velocity Oxy-Fuel (HVOF) Superalloy Coatings On Ductile Irons. Sakarya University Journal of Science, 23(2), 291-300, DOI: 10.16984/saufenbilder.465631
Access link
http://www.saujs.sakarya.edu.tr/issue/39539/465631

Sakarya University Journal of Science 23(2), 291-300, 2019

Electrochemical Corrosion Behavior of High Velocity Oxy-Fuel (HVOF) Superalloy Coatings on Ductile Irons

Yusuf Kayalı, Muhammet Karabaş* Yılmaz Yalçın, Aysel Büyüksağiş, Şükrü Talaş

ABSTRACT

In this study, alloyed and unalloyed ductile irons (DI) were coated with two different Ni-based superalloy materials by HVOF method. Microstructure and phase analyzes of the coatings were performed by using SEM, EDX, XRD methods. The electrochemical corrosion behavior of alloyed and unalloyed DI is investigated in 3.5% (w / v) NaCl solution. As a result of the characterization studies, it was observed that a dense non-porous coating layer of about 80 μm thickness was obtained on the cast iron samples and continuous adhesion was provided between the coating and the substrate. It has been determined that the cast iron coated with AMDRY 9624 contains γ matrix and β intermetallic phases and the coating produced with AMDRY 9951 commercial powder contains only γ phase. As a result of coating process, the corrosion rate of the alloyed and unalloyed spherical graphite cast irons is reduced. Also, the corrosion rate of the coating produced with AMDRY 9951 is higher than the coating produced with AMDRY 9624.

Keywords: HVOF, Ductile Iron, Electrochemical Methods, Corrosion Resistance

1. INTRODUCTION

The improvement of surface properties of commonly used cast iron in many industrial areas such as mining, agriculture, automotive and construction, will increase their strength in high temperatures and corrosive environments, they also open up their use in different areas [1,2]. One of the most common techniques for improving surface properties is coating on the material. In addition to laser, plasma and electrochemical assisted coating techniques, thermal spraying techniques are also commonly used for coating cast iron materials [3-8]. In particular, the surfaces of the rollers that are made of cast iron used in the mining and paper industries are coated with materials such as Tungsten-Carbide-Cobalt (WC-Co) which are resistant to wear by thermal spraying techniques [9,10]. Within the scope of the research and development activities directed to the automotive industry, various coatings are produced by thermal spraying techniques on aluminum-based parts manufactured by casting method and subjected to various tests [11].

MCrAlY (M: Ni, Co or Ni-Co) are applied as a bonding layer material in thermal barrier coating systems that are used in gas turbine engines [12]. These coatings are widely preferred in service conditions where high temperatures and corrosive environments. These coatings can be classified as three different types, nickel-based, cobalt-based and nickel-cobalt based. Nickel-cobalt based coating material should be used in environments where resistance to oxidation in high temperature gas environment is required to be nickel-based (M: Nickel) and cobalt-based environments where resistance against hot gas corrosion is required

* Corresponding Author: mkarabas@itu.edu.tr

and where both oxidation and corrosion resistance are required [13-15]. These metallic based coatings can be successfully applied by plasma spraying, high velocity oxy-fuel (HVOF) methods. However, the coatings produced with high-velocity oxy-fuel contain denser, less porous and less metal-oxides than those produced by plasma spraying. This is because plasma spraying has a higher particle temperature and lower particle velocity than a HVOF technique. For this reason, HVOF is known as the most suitable thermal spraying technique for production of metallic coatings [16-18].

In the HVOF technique, oxygen, air and fuel gas or liquid (propane, hydrogen, kerosene) are feed to the combustion chamber in the gun, where the mixing of the gases is ensured. Mixed and pressurized gases are ignited from a nozzle and a high-velocity flame jet is obtained. The coating powders are fed in the flame jet and the powders are warmed up, gain kinetic energy. The semi-molten and accelerating powders are sprayed onto the substrate material and the coating deposit forms [19, 20].

In this study, two different Ni-based MCrAlY powder is coated on alloyed and unalloyed cast iron by HVOF. Microstructure, phase analysis and electrochemical corrosion behavior in 3.5% (w / v) NaCl solution of the coatings are also investigated.

2. MATERIALS AND METHODS

2.1. Substrate and Coating

Alloyed and unalloyed cast iron was used as a substrate. Chemical composition of cast irons is shown in Table 1.

Table 1. Chemical composition of cast iron substrates

Substrates	C	Si	S	Mo	Cu	Mn	P	Ni
Unalloyed DI	3.85	2.273	0.01	0.001	0.044	0.141	0.048	-
Alloyed DI	3.5	2.6	0.007	0.146	0.6	0.164	0.026	1.12

Figure 1 shows microstructure of alloyed and unalloyed cast iron substrate. For unalloyed ductile iron, spherical shape graphites distributed more frequent and small size, whereas for alloyed ductile iron, graphite granules showed rougher and rarely distribution.

Nickel-based AMDRY 9624 and AMDRY 9951 powders, which are commercially available from Metco were selected as coating materials. Table 2 shows chemical composition of powders which are presented in catalog. As it can be seen in Table 2, AMDRY 9951 contains cobalt, but AMDRY 9624 does not. This difference strongly affects chemical and physical properties of coatings related to phase structure and chemical composition.

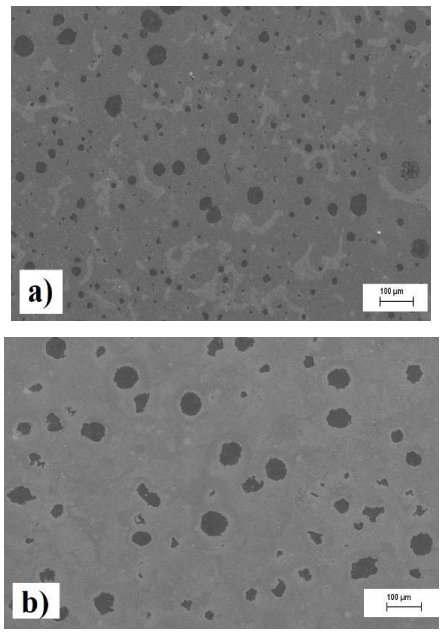

Figure 1. SEM micrographs of a) Alloyed, b) unalloyed spherical cast iron substrate

Table 2. Chemical composition of powders

Powders	Ni	Cr	Al	Co	Y_2O_3	Other	Org.
AMDRY 9624	Balance	21-23	9-11	-	0.8-1.2	-	-
AMDRY 9951	29-35	18-24	5-11	Balance	0.1-0.8	1	-

Ductile iron specimens, 10 mm in diameter, 15 mm in thickness, were grit blasted using 50-80 mesh alumina particles in order to remove surface oxides and to improve adhesion of coatings. After the grit blasting, cast iron samples were cleaned with ultrasonic cleaner for 30 minutes in technical ethanol in order to remove surface contamination occurred during sandblasting process.

HVOF gun were fastened on a three-axis CNC table and gun speed was selected as 200 mm/min. Grit blasted samples were fixed by using clamps on the turntable. Its speed was selected as 50 Hz and the number of coating passes was selected as 12. An Amdry 9951 and 9624 powder was sprayed for coating production by using Metco DJ2700 HVOF gun. HVOF process parameters are listed in Table 3.

Table 3. HVOF Process Parameters

HVOF parameters	
Powder Feed Rate(gr/dk)	50
Spray Distance(mm)	250
Prophane Flow Rate(Scfh)	40
Oxygen Flow Rate(Scfh)	24
Air Flow Rate(Scfh)	50
Turntable Speed(Hz)	50
Spray Angle(°)	90

To observe the microstructure of the coatings, coated samples were cut from the center using precision cutting. After that, the samples were polished with 240, 320, 600, 1000, 1200 grit abrasive paper and 1 μm alumina polishing suspensions, respectively. The microstructure of the coatings were examined by field emission electron microscopy (SEM) which is equipped with energy dispersive x ray (EDX) spectroscopy. X-ray diffraction (Shimadzu XRD–6000, CuK_α radiation) was used to determine the phase structure of the coatings. The thickness of the coatings was measured by means of an apparatus connected to an optical microscope.

2.2. Electrochemical Corrosion Tests

Electrochemical corrosion tests were performed using Gamry reference 600 potentiostat / galvanostat ZRA. Electrochemical calculations were performed with the Echem analyst soft software program. Prior to the electrochemical corrosion tests, the specimens which were ultrasonically cleaned at 35 ° C for 15 min intervals with aceton, ethanol and double distilled water were dried at 40 °C in an oven. Corrosion rate, polarization resistance (Rp) and corrosion current (I_{corr}) values were determined from the current-potential curves. Then the corrosion current density (icorr.) was found by dividing by the surface area of the corrosion current. % inhibition value is calculated from the following formula. Where ic and i0 represent the corrosion rates of the coated and uncoated layers, respectively.

$$inhibition\ \% = \frac{io-i}{io} \times 100 \quad \text{(Equation 1)}$$

3. RESULTS AND DISCUSSION

3.1. Coating Characterization

Figure 2 and 3 show XRD pattren of two different cast iron samples and coatings. Figure 2a and 3a are XRD patterns obtained from two different cast iron surfaces before coating. All of XRD peaks belong to α-Fe phase for two types of ductile iron.

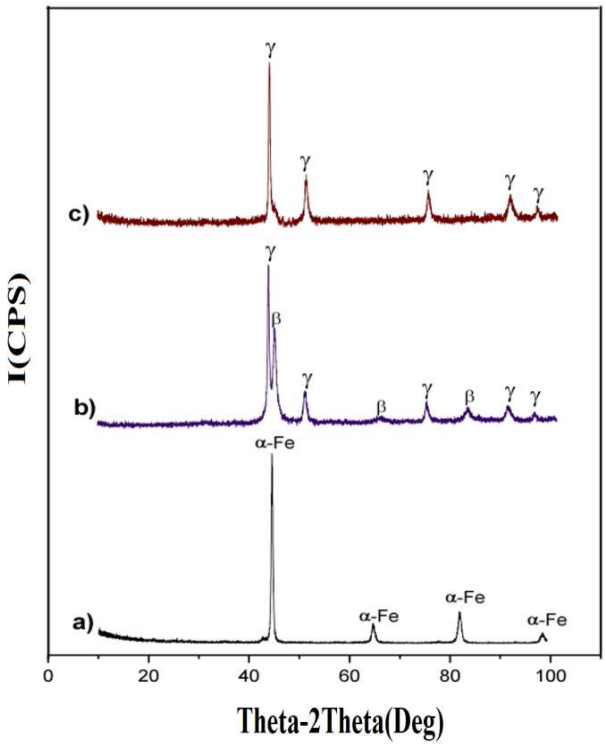

Figure 2. a) XRD pattern of Unalloyed spherical cast iron, b) 9624 coating and c) 9951 coating

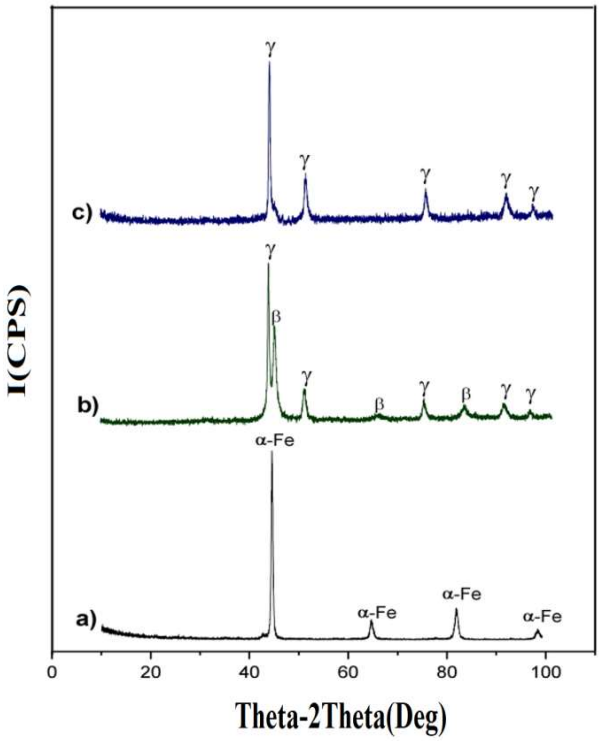

Figure 3. a) XRD pattern of alloyed spherical cast iron, b) 9624 coating and c) 9951 coating

Figure 2b and 3b show XRD pattern of coatings produced by AMDRY 9624 powder. According to these XRD patterns, the coatings produced by the AMDRY 9624 consist of two different phases, β and γ. The β phase is intermetallic compounds made by Ni and Co elements alone or together with Al and is a body centered cubic (BCC) structure. The γ phase is a solid solution of Co, Ni, Cr, etc. and is a face centered cubic (FCC) structure [17, 18].

Figures 2c and 3c show XRD pattern of coatings produced by AMDRY 9951 powder. It was determined that the coating contains a single phase and this phase is named as γ solid solution. The XRD peak of the β intermetallic compounds was not found for the AMDRY 9951 coating. It is indicated that solidification behavior and powder particle-flame jet interaction is different for two types of feedstock [21, 22].

Figure 4 shows cross-sectional SEM image of coatings on unalloyed cast iron substrate. Spherical shaped graphite distributed randomly in cast iron substrate is clearly seen in cast iron base material. For both coatings, the coating thickness is measured as approximately 80 μm. There is no problem in the adhesion of the coating layer to the substrate. As a result of the coating process, a dense and continuous coating layer was obtained. However, the presence of very few porous zones in the coating microstructure is remarkable [23].

Figure 5 shows a cross-sectional SEM image of the coatings on alloyed cast iron substrate fabricated by HVOF using AMDRY 9624 and 9951 feedstock. A continuous, dense and very low-porosity coating layer was obtained for both coatings [24]. However, cracks were formed in the coating-substrate interface region. These cracks are thought to be due to the process of metallographic sample preparation, as well as the expansion and contraction caused by the heating and cooling of the cast iron substrate during the HVOF process [25].

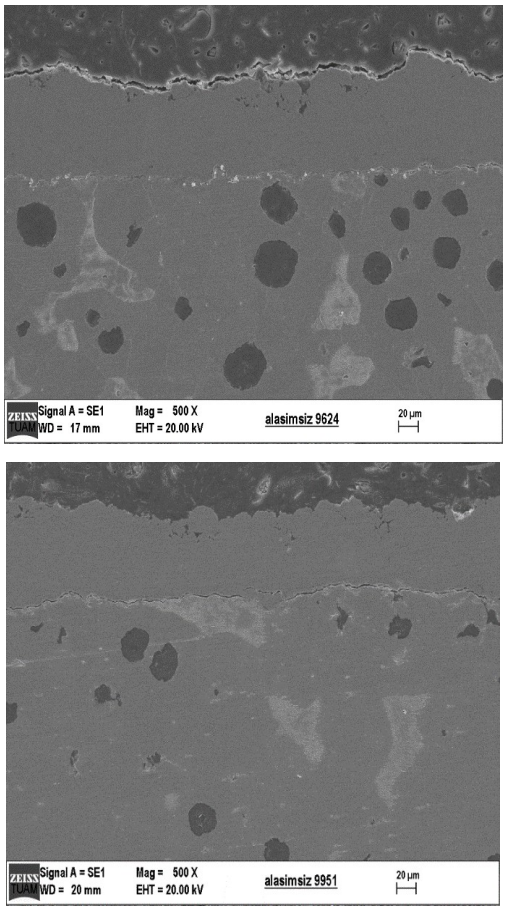

Figure 4. SEM images of a) 9624 coating, b) 9951 coating on unalloyed spherical cast iron substrate

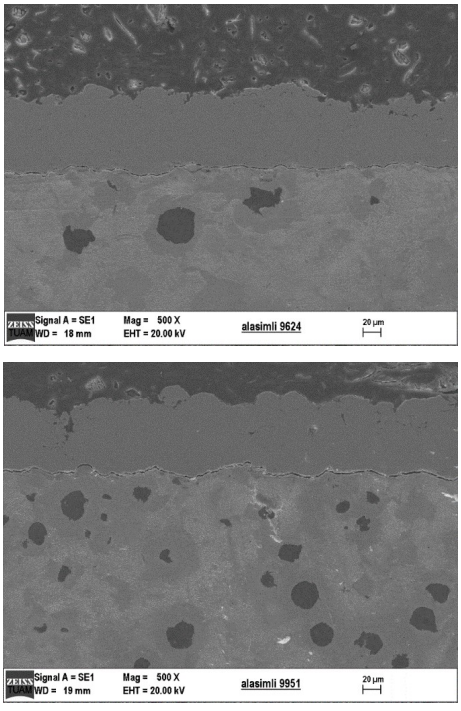

Figure 5. SEM images of a) 9624 coating, b) 9951 coating on alloyed spherical cast iron substrate

3.2. Electrochemical Corrosion Behaviors of Coating

Corrosion characteristics from extrapolation Tafel curves are given Table 4. Tafel plots are given at Figure 6, for the coated and uncoated ductile irons in 3.5% (w/V) NaCl after an hour waiting period.

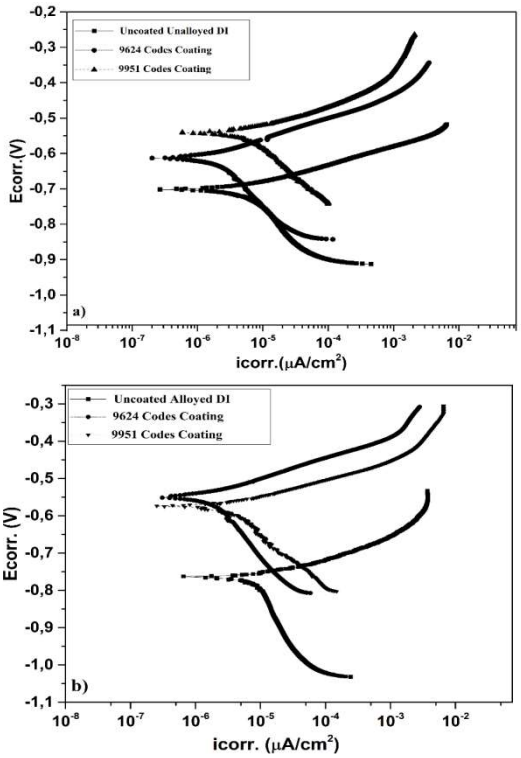

Figure 6. Tafel plots in 3.5% NaCl solution a) Unalloyed and b) Alloyed ductile iron

When Table 4 is examined, the corrosion current density (i_{Corr}) values of the coated samples are reduced after an hour in 3.5 % (w / v) NaCl medium. The values of the polarization current density are 5,490 µA / cm^2 for uncoated non-alloyed SGCI, while the polarization current density values for coated samples vary between 1,960-3,710 µA / cm^2 depending on the nature of the coating. For alloyed SGCI, corrosion rate is 8,960 µA / cm^2 whereas for coated samples the polarization current density value varies between 1,960-3,230 µA/ cm^2 depending on the characteristics of the coating. The corrosion resistance of the coated specimens increased with the coating layer formed [26]. It is also observed that Rp (polarization resistance) and corrosion rate values (mpy) are in agreement with the i_{Corr} values. As i_{corr} value increases, Rp value and % inhibition value decrease.

Table 4. Corrosion Characteristics of Unalloyed and Alloyed Ductile Iron.

Solution	Substrate	Sample	icorr. ($\mu A/cm^2$)	Ecorr. (mV)	Corr. Rate (mpy)	Rp (kΩ)	Inhibition %
3.5 % NaCl	Unalloyed DI	Uncoated	5.49	-702	3.146	1.419	-
		AMDRY 9624	1.96	-613	1.123	2.813	64.3
		AMDRY 9951	3.71	-568	2.127	1.724	32.42
	Alloyed DI	Uncoated	8.96	-565	5.141	1.036	-
		AMDRY 9624	1.69	-550	1.124	4.153	78.125
		AMDRY 9951	3.23	-574	1.852	1.601	63.95

The corrosion rate of unalloyed ductile iron is higher than the corrosion rate of uncoated alloys. Because on the surface has spherical graphite and Fe_3C on the ferritic matrix. Since the surface is uncoated, the Cl^- ions diffuse through the surface of unalloyed ductile iron and form complexes (such as $FeCl_3$, $FeCl^-$, etc.) that dissolve with the Fe^{2+} ion, increasing the surface corrosion.The Ecorr value shifs to be at more negative potentials. This indicates that the cathodic reaction is effective on corrosion and that the oxygen present in the solution is cathodically reduced. As long as the cathodic reaction continues, the material will corrode because the need for electrons will lead to the oxidation reaction of iron in the unalloyed ductile iron. The cathodic reaction takes place by reducing the metals to hydroxyl ions of oxygen molecules dissolved in poor, neutral and basic environments in terms of hydrogen ions [27].

This phenomenon, which is defined as the oxygen reaction,

Cathodic reaction: $O_2 + 2H_2O + 4é \rightarrow 4OH^-(aq)$ (Equation 2)

In order for this reaction to occur, dissolved oxygen must reach the metal surface by diffusion of the molecules. The damage of steel parts and structures in seawater is the most common example of the corrosion caused by the oxygen reaction. A neutral 3.5 % NaCl (artificial sea water) solution is in constant contact with the air at the same time. The anodic reaction can be given as:

Anodic reaction: $Fe(s) \rightarrow Fe^{2+}(aq) + 2é$ (Equation 3)

Total reaction : $Fe(s) + 2H_2O(l) + O_2(g) \rightarrow 2Fe(OH)_2(s)$ (Equation 4)

Over time Iron (II) hydroxide forms and is converted into the iron (III) hydroxide, which we know to be the rust i.e. the reaction is:

$2Fe(OH)_2(s) + H_2O(l) + ½\ O_2(g) \rightarrow 2Fe(OH)_3(s)$ (Equation 5)

AMDRY 9624 code and AMDRY 9951 code coatings have reduced corrosion rate. The chemical composition of AMDRY 9624 has been effective in preventing corrosion. In particular, nickel present in composition of AMDRY9624 has reduced the corrosion rate by forming nickel oxides. Ecorr values of coated

AMDRY9624 samples shift the more positive potentials, this shows to form the anodic reactions on the surface prevent corrosion. The coating elements on the surface form oxide and hydroxide (Equation 4-5). These oxide and hydroxides formed on the surface act as a barrier film, preventing Cl ion diffusion [28-30]. The resulting passive layer reduces the dissolution of the metal and protects the metal [31]. The iron is given three different oxide layers depending on the partial pressure of O_2 in air. For this reason, the oxidation of iron is a bit complicated. The oxygen rich layer is found in the outer oxide layer. The most important elements that improve iron oxidation resistance are Cr and Al. The oxidation resistance of Cr-Fe alloys is good.

Corrosion rate of unalloyed AMDRY 9951 coded coated sample is higher than the corrosion rate of non-alloyed AMDRY 9624 coded coating. The amount of nickel and Y_2O_3 in the structure of AMDRY 9951 coded coating is less. Although cobalt is in equilibrium, it has not been effective in preventing corrosion. Cobalt does not have reactivity to react with air. But when it is heated it forms an oxide of Co_3O_4. If the reaction takes place at 900 ° C, cobalt (II) oxide (CoO) is formed. It does not react directly with nitrogen in the air.

$$3Co(s) + 4O_2(g) \rightarrow 2Co_3O_4(s) \quad \text{(Equation 6)}$$

$$2Co(s) + O_2(g) \rightarrow 2CoO(s) \quad \text{(Equation 7)}$$

The cobalt metal is not a very reactive element against water. But at the red temperature (900 ^oC), cobalt (II) oxide (CoO) is formed the reaction between cobalt metal and water vapor.

$$2Co(s) + O_2(g) \rightarrow 2CoO(s) \quad \text{(Equation 8)}$$

Owing to these properties of cobalt, no oxide has formed on the surface. It has undergone corrosion like unalloyed ductile iron. The AMDRY 9951 coating formed on the surface prevented corrosion to some extent. The oxides formed by nickel in the find AMDRY 9951 composition also partially reduced corrosion. The low content of Y_2O_3 in the AMDRY 9951 coded coating also increased the corrosion.

When Figures 7 and 8 are examined, the chloride ions on the surface of the alloyed ductile iron are 6 times more than the chloride on the surface of the unalloyed ductile iron. As the chloride ions are very aggressive and the creating iron-soluble salt complexes, the corrosion rate of the alloyed ductile iron is higher. Oxygen and iron on the surface may react with each other form oxides and hydroxides. When EDX% atomic ratios (Fe and O) values are compared, $Fe(OH)_3$ may be considered to be formed on the alloyed surface. The increase in nickel, cobalt, aluminum and chromium levels on the surface of AMDRY 9951 coded coating has been effective in reducing the corrosion and the decrease of chlorine on the surface has been effective in reducing the corrosion.

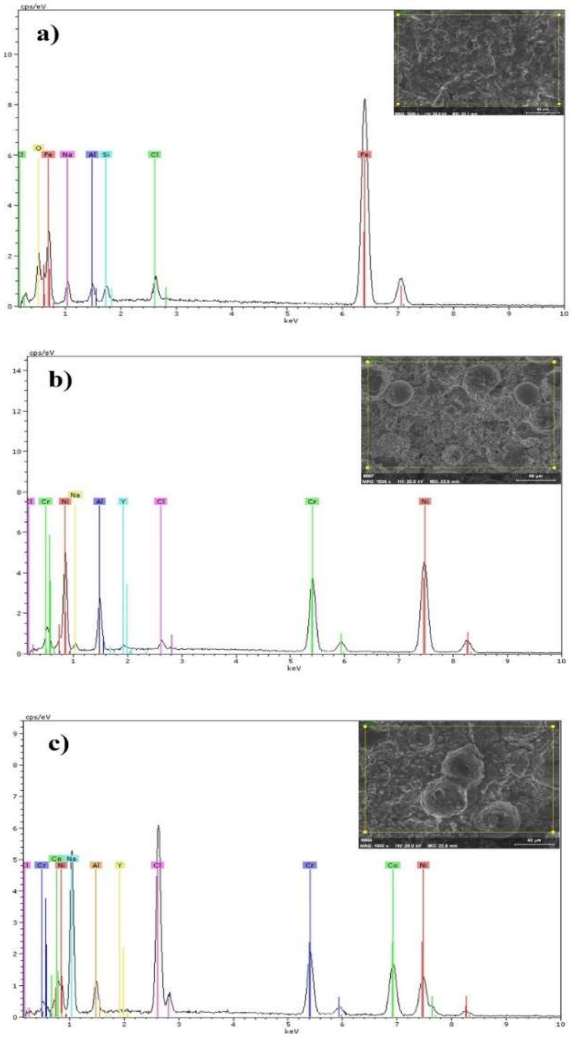

Figure 7. SEM-EDX analyzes after corrosion tests a) unalloyed, b) 9624 coded coating ductile iron and c) 9951 coded coating ductile iron

In AMDRY 9951 and AMDRY 9624 coded coatings, the absence of Fe and Si on the surface of unalloyed and alloyed ductile irons indicates that the surfaces of ductile irons are completely covered. It showed that the coatings were successful.

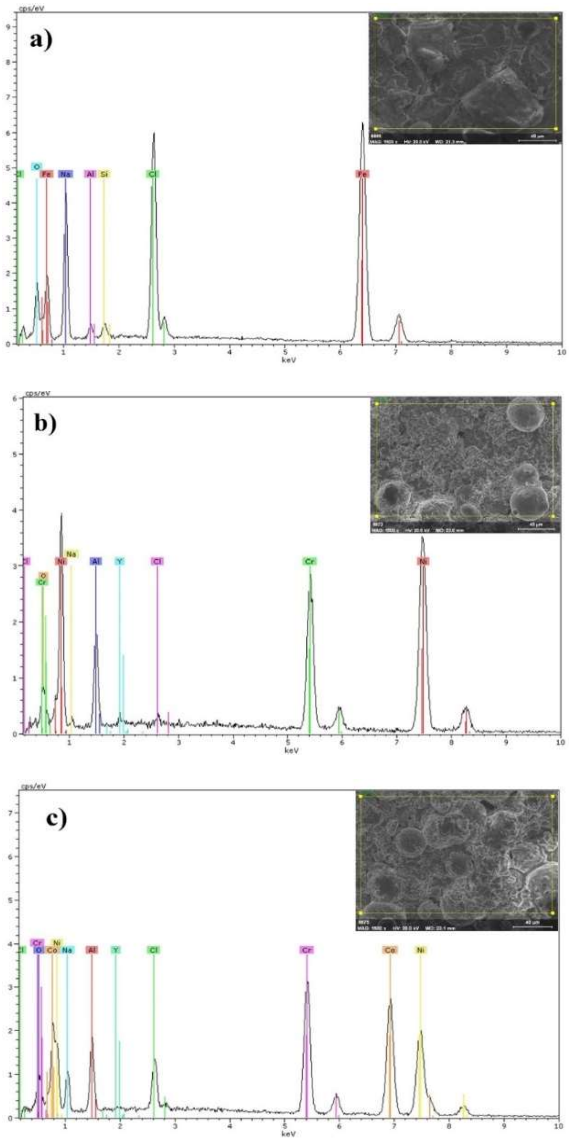

Figure 8. EDX analyzes after corrosion tests a) unalloyed, b) 9624 coded coating ductile iron and c) 9951 coded coating ductile iron

4. RESULTS

The following conclusions can be drawn from this study:

Alloyed and unalloyed spherical graphite cast iron were successfully coated with the two different Ni-based MCrAlY feedstock by the HVOF method. A dense, porosity-free coating layer of about 80 μm thickness was obtained on cast iron substrate and continuous adhesion between the coating and the substrate was achieved. γ and β phase and only γ phase were obtained by XRD analysis for AMDRY 9624 and AMDRY 9951 feedstock respectively.

In the electrochemical corrosion tests, the corrosion current density is 5,490-8,960 μA / cm^2 in the uncoated alloyed and unalloyed spherical cast iron substrate respectively, whereas in the coated samples the polarization current density value varies from 1,960-3,710 μA / cm^2 depending on the characteristics of the coating. The corrosion resistance of the spherical cast iron substrate samples increased with the coating layer formation. With these two different coatings, the inhibition values of spherical cast iron samples were up to 78%. The amount of nickel in the coating material has been a factor in the reduction of corrosion.

ACKNOWLEDGMENTS

The authors are grateful to the Scientific Research Project Council of Afyon Kocatepe University (Project Number: 17. KARİYER.231).

REFERENCES

[1] R., Singh, “Cast Iron Metallurgy. Materials Performance”, 48 (9), pp. 58-61, 2009.

[2] R., O'Rourke, “Cast Iron: The engineered metal”, Advanced Materials Processes, 159 (1), pp. 65-68, 2001.

[3] J.L., Liu, G.Q., Shi, P.D., Ding, H.O., Ye, Z.X., Ou, “Features of laser alloying of grey cast iron”, Lasers in Engineering, 6(2), pp. 81-101, 1997.

[4] X., Cheng, S.B., Hu, W.L., Song, X. S., Xiong, “Improvement in corrosion resistance of a nodular cast iron surface modified by plasma beam treatment”, Applied Surface Science, 286, pp. 334-343, 2013.

[5] Z., Lestan, M., Milfelner, J., Balic, M., Brezocnik, I., Karabegovic, “Laser deposition of Metco 15E, Colmony 88 and VIM CRU 20 powders on cast iron and low carbon steel”, International Journal of Advanced Manufacturing Technology, 66(9-12), pp. 2023-2028, 2013.

[6] A.L. Maco and F.J. Belzunce, “Laser surface hardening of gray cast irons”, Revista De Metalurgia, 34(2), pp. 126-130, 1998.

[7] V., Ozcelik, U., Oliveira, M., Boer, J.T.M., Hosson, “Thick Co-based coating on cast iron by side laser cladding: Analysis of processing conditions and

coating properties", Surface & Coatings Technology, 201(12), pp. 5875-5883, 2007.

[8] F., Fernandes, A., Cavaleiro and A., Loureiro, "Oxidation behavior of Ni-based coatings deposited by PTA on gray cast iron", Surface & Coatings Technology, 207, pp. 196-203, 2012.

[9] P., Fauchais and A., Vardelle, "Thermal sprayed coatings used against corrosion and corrosive wear, in Advanced plasma spray applications", InTech. 2012.

[10] J., Yoganandh, S., Natarajan and S.P.K., Babu, "Erosion Behaviour of WC-Co-Cr Thermal Spray Coated Grey Cast Iron under Mining Environment", Transactions of the Indian Institute of Metals, 66(4), pp. 437-443, 2013.

[11] J., Vetter, G., Barbezat, J., Crummenauer, J. Avissar, "Surface treatment selections for automotive applications", Surface and Coatings Technology, 200(5), pp. 1962-1968, 2005.

[12] I.G., Wright and B.A., Pint, "Bond coating issues in thermal barrier coatings for industrial gas turbines", Proceedings of the Institution of Mechanical Engineers Part a-Journal of Power and Energy, 219(A2), pp. 101-107, 2005.

[13] Y., Itoh, M. Saitoh M. Tamura, "Characteristics of MCrAlY coatings sprayed by high velocity oxygen-fuel spraying system", Journal of Engineering for Gas Turbines and Power-Transactions of the Asme, 122(1), pp. 43-49, 2000.

[14] Z.W., Huang, Z.G., Wang, S.J., Zhu, F.H., Yuan, F. G., Wang, "Effect of HVOF sprayed MCrAlY coating on thermomechanical and isothermal fatigue life of superalloy M963", Surface Engineering, 23, pp. 373-374, 2008.

[15] M., Seiersten and P. Kofstad, "Sodium Vanadate-Induced Corrosion of Nickel and Mcraiy Coatings on Inconel-600", Materials Science and Technology, 3(7), pp. 576-583, 1987.

[16] S.V., Joshi and R. Sivakumar, "Particle Behavior during High-Velocity Oxy Fuel Spraying", Surface & Coatings Technology, 50(1), pp. 67-74, 1991.

[17] J.R., Davis, "Handbook of thermal spray technology", ASM international, 2004.

[18] M. Shibat, S., Kuroda, M., Watanabe, Y., Sakamoto, "Oxidation property of CoNiCrAlY coatings prepared by various thermal spraying techniques", High-Temperature Oxidation and Corrosion, 522-523, pp. 339-344, 2006.

[19] P.S. Grewal, V., Chawla and J.S., Grewal, "High Velocity Oxy-fuel Sprayed Coatings- a Review", Journal of the Australian Ceramic Society, 47(2), pp. 30-36, 2011.

[20] J., Koutsky, "High Velocity Oxy-Fuel spraying", Journal of Materials Processing Technology, 157, pp. 557-560, 2004.

[21] S., Saeidi, K.T., Voisey and D.G., McCartney, "Mechanical Properties and Microstructure of VPS and HVOF CoNiCrAly Coating", Journal of Thermal Spray Technology, 20(6), pp. 1231-1243, 2011.

[22] S., Saeidi, K.T., Voisey and D.G., McCartney, "The Effect of Heat Treatment on The Oxidation Behavior of HVOF and VPS CoNiCrAly Coating", Journal of Thermal Spray Technology, 18(2), pp. 209-216, 2009.

[23] K., Fritscher and Y.T., Lee, Investigation of an as-sprayed NiCoCrAlY overlay coating microstructure and evolution of the coating. Materials and Corrosion-Werkstoffe und Korrosion, 56(1), pp. 5-14, 2005.

[24] C.T., Kwok, P.K., Wong, F.T., Cheng, H.C., Man, **"**Characterization and corrosion behavior of hydroxyapatite coatings on Ti6Al4V fabricated by electrophoretic deposition", Applied Surface Science, 255, pp. 6736–6744, 2009.

[25] A.L.A., Escada, D., Rodrigues, J.P.B., Machado, A.P.R., Alves Claro, "Surface characterization of Ti–7.5Mo alloy modified by biomimetic method", Surface & Coatings Technology, 205, pp. 383–387, 2010.

[26] G.K., Kariofillis, G.E., Kiourtsidis, D.N. Tsipas, "Corrosion behavior of borided AISI H13 hot work steel", Surface & Coatings Technology 201, pp. 19–24, 2006.

[27] H.H., Uhlig (Ed.), "Corrosion Handbook", second ed., John Wiley & Sons, New York, 2000.

[28] M.M., Verdian, K., Raeissi, M., "Salehi, Characterization and electrochemical properties of Ni(Si)/Ni_5Si_2 multiphase coatings prepared by HVOF spraying", Applied Surface Science, 261, pp. 493–498, 2012.

[29] A., Balamurugan, G., Balossier, S., Kannan, J., Michel, J., Faure, S., Rajeswari, "Electrochemical and structural characterization of zirconia reinforced hydroxyapatite bioceramic sol-gel coatings on surgical grade 316L SS for biomedical applications", Ceramics International, 33, pp. 605-614, 2007.

[30] S., Kannan, A., Balamurugan, S., Rajeswari, "H_2SO_4 as a passivating medium on the localised corrosion resistance of surgical 316L SS metallic implant and its effect on hydroxyapatite coatings", Electrochimica Acta, 49, pp. 2395-2403, 2004.

[31] H.N., Cheng, R.A., Gross, "Polymer Biocatalysis and Biomaterials", ACS Symposium, 900, pp. 560, 2005.